Academy for Global Science and Innovation (AGSI)

ARTICLE

Solubility-Aware Reduced-Order State Estimation for Real-Time Gas Kick Detection and Control from Surface Measurementss

Le Quoc Truong[1] and Tran Minh Kiet[2]

[1]Thai Nguyen University of Information and Communication Technology, Z115 Road, Quyet Thang Ward, Thai Nguyen City 250000, Vietnam
[2]University of Khanh Hoa, 01 Nguyen Chanh Road, Nha Trang City 650000, Vietnam

Abstract

Gas influx events during drilling remain a principal source of nonproductive time and a persistent precursor to loss-of-well-control incidents. Modern rigs provide dense surface instrumentation, yet the mapping from surface pressure and flow signals to evolving downhole multiphase states is often nonunique because of coupled effects from compressibility, slip, friction, temperature variation, and transient boundary conditions. This paper develops a solubility-aware, reduced-order digital twin and a Bayesian state-estimation scheme that jointly infer kick onset, influx mass, and migration dynamics using only surface measurements and routine rig telemetry. The core modeling contribution is a thermodynamically consistent partition of the influx gas between dissolved and free phases, coupled to a drift-flux-based annular momentum closure and a temperature-dependent equation of state, enabling fast evaluation without solving full-field computational fluid dynamics. The inference contribution is a sequential probabilistic filter that propagates uncertainty through the reduced-order dynamics while assimilating standpipe/choke pressures, pit volume, and pump-rate data, yielding posterior distributions over kick size and location rather than point estimates. A regime-aware closure is introduced through a constrained, differentiable surrogate for friction and slip that preserves physical monotonicity and mass conservation, allowing robust operation across shut-in and circulating conditions. Numerical experiments over a broad range of depths, mud properties, and influx scenarios demonstrate that incorporating dissolution reduces systematic bias in inferred influx volume and improves early-warning reliability under realistic sensor noise. The resulting framework is designed for real-time use, emphasizing identifiability, bounded computational complexity, and control-relevant outputs.

1. Introduction

Gas kicks are intrinsically transient, multiscale phenomena that couple reservoir inflow, annular multiphase transport, thermodynamic phase behavior, and surface-control actions [1]. The operational need is deceptively simple: detect an influx early, estimate its magnitude and type, and choose choke and pump actions that restore overbalance while staying within surface and downhole pressure constraints. The scientific difficulty is that the measurements most readily available to the driller are not direct observations of the downhole multiphase state; instead, they are filtered through a distributed, evolving hydraulic system whose response depends on geometry, mud rheology, gas compressibility, slip, and thermal gradients. Even when high-frequency surface data are available, multiple downhole state trajectories can produce similar surface signatures, particularly during the early stage of an event when gas holdup is small and the system is still close to nominal circulation.

A central limitation of many real-time kick-response tools is the separation of detection from

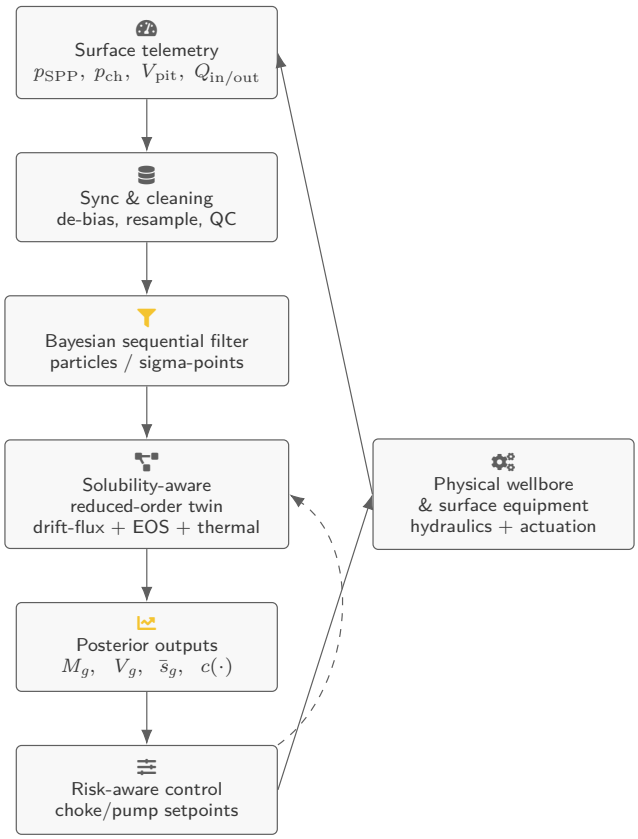


Figure 1. Real-time architecture: surface measurements are assimilated by a Bayesian filter wrapped around a solubility-aware reduced-order digital twin. The estimator produces posterior distributions over kick size, dissolved/free partition, and migration state; the control layer evaluates candidate choke/pump actions under uncertainty to maintain pressure constraints while circulating out the influx.

dynamics [2]. Threshold rules flag flow-out or pit gain deviations, while subsequent calculations assume simplified hydraulics or steady-state pressure gradients. These approaches are vulnerable to false positives from operational transients, as well as false negatives when dissolution or delayed gas breakout masks early pit gain. At the same time, fully resolved transient multiphase simulators exist, but their computational cost and calibration burden often exceed what is feasible in field decision windows. The practical gap suggests a modeling target that is neither purely empirical nor fully resolved: a reduced-order mechanistic model that is fast, identifiable from surface measurements, and expressive enough to represent the main nonlinearities that govern early signal formation.

Surface pressure provides a particularly valuable diagnostic channel because it is continuously observed, synchronized with pump controls, and directly linked to the integrated annular momentum balance [3]. Recent laboratory evidence has shown that surface pressure responses can be systematically associated with annular flow regimes and kick evolution under circulating conditions, motivating the idea that surface pressure can serve as a primary detection and characterization signal when interpreted through an appropriate model [4]. However, a purely data-driven mapping from surface pressure to regime or kick size risks brittleness under

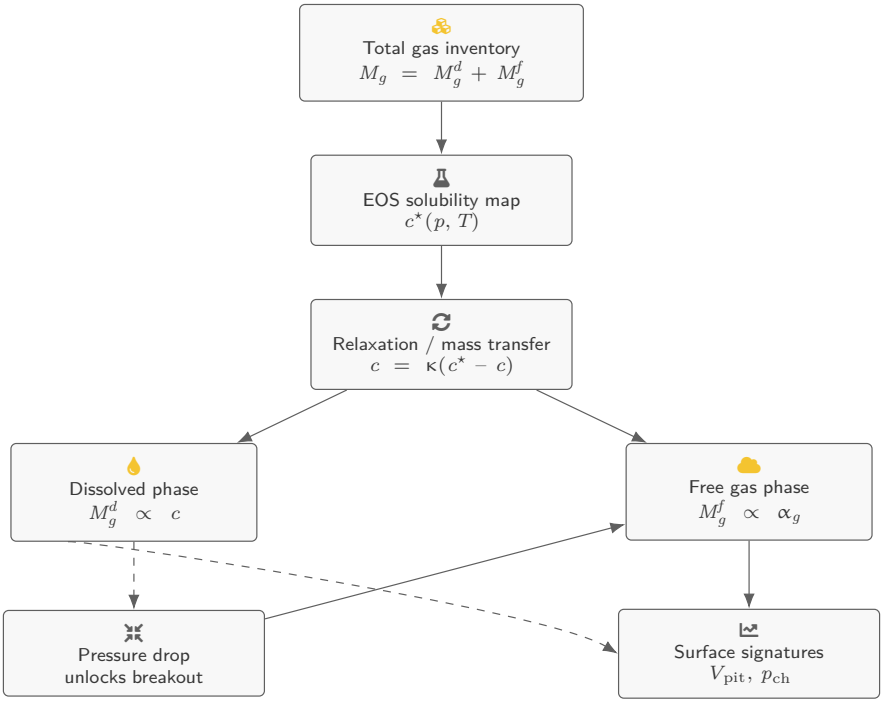


Figure 2. Thermodynamically structured dissolved/free partition used for real-time inference. An EOS-derived solubility target $c^\star(p, T)$ governs how total gas inventory splits into dissolved gas M_g^d and free gas M_g^f through a bounded relaxation model. Pressure changes shift equilibrium and can rapidly convert dissolved inventory into free gas, altering pit gain and casing/choke pressure trajectories even when early free-gas indicators are weak.

changes in geometry, fluid properties, and temperature, while a purely mechanistic mapping risks bias if critical physics, such as dissolution in nonaqueous muds, is neglected.

This paper advances a unified framework in which a solubility-aware reduced-order annular model is embedded within a Bayesian sequential inference architecture. The thesis is that real-time well-control decisions can be materially improved by treating kick characterization as an online inverse problem with quantified uncertainty, where a physically constrained state-space model maps controls and boundary conditions to surface observables [5]. The technical contribution is not a synthesis of prior kick studies, but an integrated modeling and inference methodology that emphasizes identifiability, computational tractability, and control relevance. The model combines (i) a mechanistic two-phase transport core with slip, compressibility, and distributed friction, (ii) a thermodynamic partitioning of gas between dissolved and free phases coupled to temperature and pressure, and (iii) a regime-aware closure that can be learned from data while enforcing conservation and monotonicity constraints. The inference layer (iv) assimilates surface telemetry through a sequential filter that produces posterior distributions over influx mass, location, and migration rate, enabling risk-aware control actions rather than deterministic heuristics.

The remainder of the paper is organized as follows [6]. A system-level state-space representation is developed, including measurement operators that connect downhole states to surface pressures and pit volume. A reduced-order multiphase dynamics model is introduced, emphasizing stable discretization and bounded computational complexity. A thermodynamic

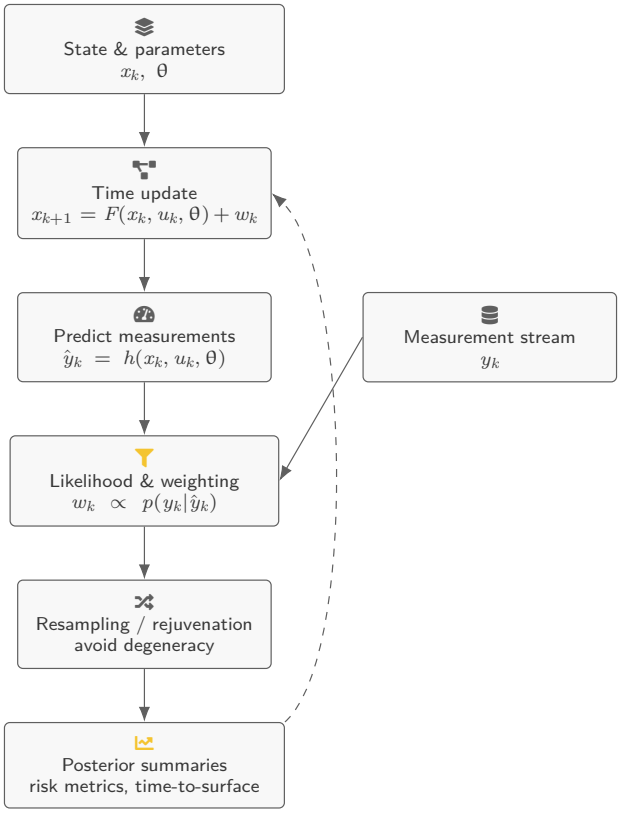


Figure 3. Bayesian sequential inference loop embedded around the reduced-order twin. Particles (or sigma-points) propagate uncertainty through nonlinear multiphase dynamics, predict surface measurements, and update weights via the multi-sensor likelihood. Resampling and mild rejuvenation maintain diversity during kick onset and regime transitions, yielding posterior distributions over influx magnitude, location, and dissolved/free inventories.

solubility closure is derived and coupled to the hydraulic core, highlighting its role in delaying breakout and altering pit gain and pressure signatures. A Bayesian filtering strategy is then constructed to solve the online inverse problem, followed by a regime-aware, physics-constrained surrogate closure to handle friction and slip across operating modes. The paper concludes with control-relevant outputs and numerical experiments that illustrate how solubility and uncertainty quantification change operational decisions [7].

2. System and Measurement Model

Consider a wellbore annulus of measured depth coordinate $s \in [0, L]$, with $s = 0$ at the bit and $s = L$ at the surface. The annulus cross-sectional area is $A(s)$ and hydraulic diameter is $D_h(s)$, both possibly varying with depth due to casing and open-hole sections. The drilling fluid is treated as a liquid phase with density $\rho_\ell(p, T)$ and effective viscosity $\mu_\ell(\gamma, T)$, while the influx is a compressible gas phase with density $\rho_g(p, T)$ and viscosity $\mu_g(T)$. The phases occupy local volume fractions $\alpha_g(s, t)$ and $\alpha_\ell(s, t) = 1 - \alpha_g(s, t)$, with superficial velocities $u_g(s, t)$ and $u_\ell(s, t)$, and mixture velocity $u_m(s, t) = \alpha_g u_g + \alpha_\ell u_\ell$. The objective is to infer, online, the evolving downhole state $x(t)$ from surface measurements $y(t)$ and known controls $u(t)$, where

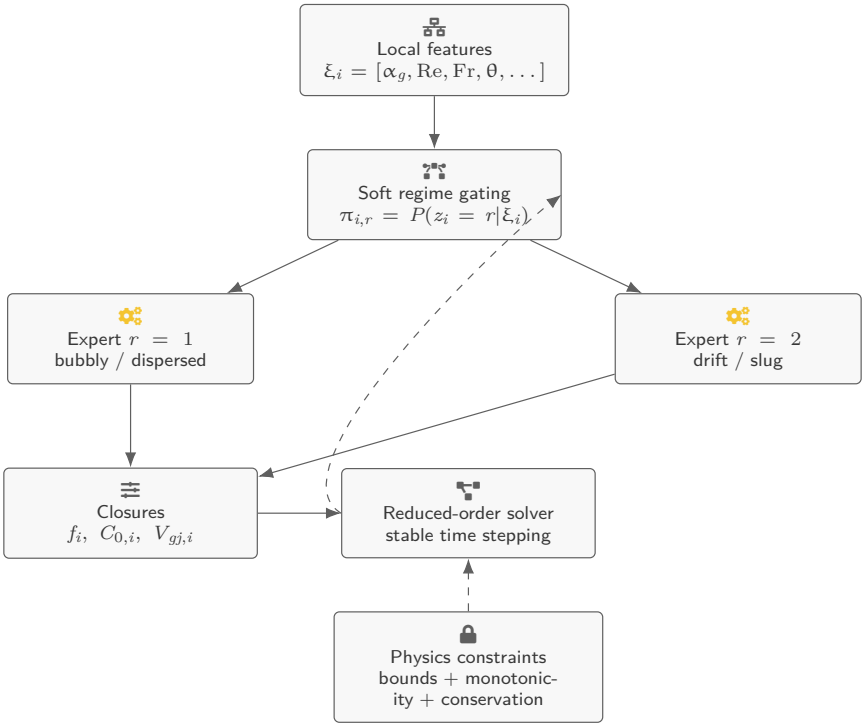


Figure 4. Regime-aware differentiable surrogate closure integrated with the reduced-order dynamics. A compact feature vector drives a soft gating model over a small set of regime experts whose outputs blend into friction and slip closures. Constraint mechanisms enforce boundedness and conservation-compatible behavior, improving stability when the estimator must explain surface pressure changes across circulating and shut-in conditions.

the controls include pump rate, choke opening, and potentially backpressure setpoint.

A practical field implementation must balance fidelity and identifiability [8]. The distributed multiphase flow problem is naturally expressed as a set of coupled partial differential equations in s and t, but this level of detail is typically underdetermined by surface-only measurements. The approach here is to define a reduced-order state vector that captures the dominant degrees of freedom governing surface signals during a kick. One effective representation aggregates the annulus into N axial cells, with cell-averaged pressure $p_i(t)$, gas void fraction $\alpha_{g,i}(t)$, mixture temperature $T_i(t)$, and a dissolved-gas state variable $c_i(t)$ representing the amount of gas in solution per unit liquid volume. The full state vector is then

$$x(t) = \left[p_1(t), \ldots, p_N(t),\ \alpha_{g,1}(t), \ldots, \alpha_{g,N}(t),\ T_1(t), \ldots, T_N(t),\ c_1(t), \ldots, c_N(t)\right]^\top, \tag{2.1}$$

with additional scalar states for influx source strength and location when needed [9]. This state choice is designed to preserve the ability to predict surface pressure and pit gain while avoiding unobservable fine-scale fields.

The governing reduced-order dynamics are obtained by integrating conservation laws over each cell. For the mixture mass balance, assuming no significant compressibility of the liquid phase over short time windows and treating gas compressibility explicitly, a cell-average mixture continuity equation can be written in terms of volumetric flow rates $Q_{m,i}(t) = A_i u_{m,i}(t)$ and sources at the boundaries. The gas mass balance must account for both free gas and dissolved

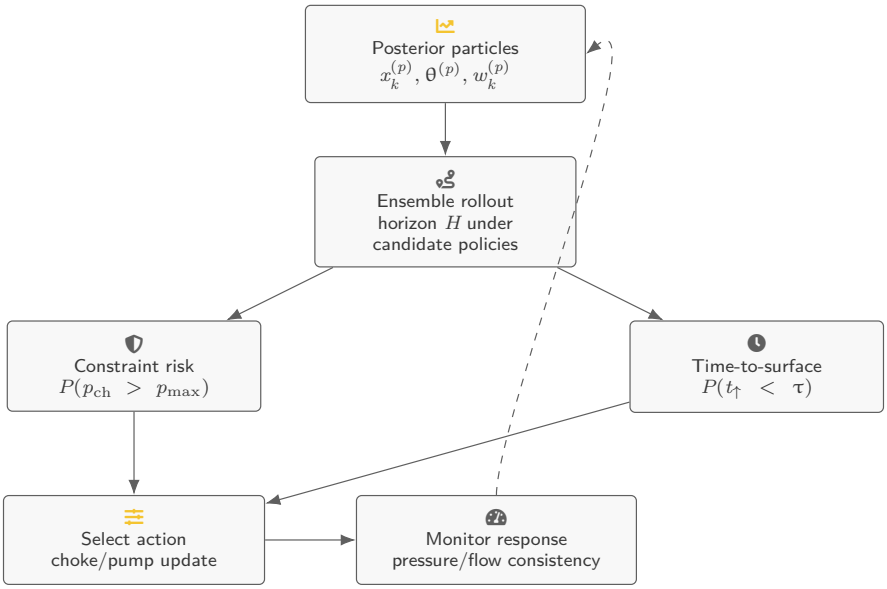


Figure 5. Control-relevant decision support from posterior ensembles. The estimators particle set is rolled forward under a small menu of candidate choke/pump policies to quantify risk of pressure-limit violation and forecast time-to-surface. Actions are selected by trading off constraint risk against migration/expansion outcomes, then validated by immediate surface-response consistency as new telemetry arrives.

gas. Let $M^f_{g,i}(t)$ denote the free-gas mass in cell i and $M^d_{g,i}(t)$ the dissolved-gas mass. Then the total gas mass is $M_{g,i}(t) = M^f_{g,i}(t) + M^d_{g,i}(t)$, and its evolution is driven by axial transport plus influx at the reservoir entry cell k:

$$\frac{dM_{g,i}}{dt} = m_{g,i-1\to i} - m_{g,i\to i+1} + \delta_{ik}\, m_{g,\mathrm{in}}(t). \tag{2.2}$$

A key modeling element is that the partition between $M^f_{g,i}$ and $M^d_{g,i}$ is not arbitrary; it is constrained by phase equilibrium and mass-transfer time scales. For real-time inference, an equilibrium or quasi-equilibrium assumption is often appropriate for small bubbles in a well-mixed cell over the time scale of minutes, while still allowing delayed breakout due to pressure changes. Accordingly, the dissolved state $c_i(t)$ is treated as a dynamic variable that relaxes toward an equilibrium solubility $c_i^\star(p_i, T_i)$ with a finite rate κ_i: [10]

$$\frac{dc_i}{dt} = \kappa_i\big(c_i^\star(p_i, T_i) - c_i\big) + \text{transport terms}. \tag{2.3}$$

This relaxation model provides a controlled way to represent non-instantaneous dissolution without introducing detailed interfacial area dynamics that are rarely observable in the field.

Momentum balance provides the link from downhole states to surface pressures. For each cell, an integrated steady-in-space, unsteady-in-time momentum approximation is used, in which pressure drop is related to acceleration, hydrostatic head, and friction. The cellwise pressure gradient can be written as

$$\frac{p_{i+1} - p_i}{\Delta s_i} = -\rho_{m,i} g \cos\theta_i - \frac{f_i \rho_{m,i} u_{m,i} |u_{m,i}|}{2D_{h,i}} - \rho_{m,i} \frac{du_{m,i}}{dt}, \tag{2.4}$$

Table 1. Key notation for the annular geometry and multiphase state variables.

Symbol	Description	Units	Type / role
s	Measured depth coordinate	m	Independent spatial coordinate along annulus
L	Total measured depth	m	Upper bound of $s \in [0, L]$ (surface at $s = L$)
$A(s)$	Annular cross-sectional area	m^2	Varies with casing / open-hole geometry
$D_h(s)$	Hydraulic diameter	m	Geometric parameter for friction correlations
$\alpha_g(s,t)$	Gas volume fraction	–	Local free-gas holdup in the annulus
$u_m(s,t)$	Mixture velocity	m/s	Volume-fraction-weighted phase velocities
$x(t)$	Reduced-order state vector	–	Stacked pressures, holdup, temperature, dissolution

Table 2. Main model and inference components in the proposed framework.

Component	Domain	Brief description
Solubility-aware partition	Thermodynamics	EOS-based split between dissolved and free gas constrained by phase equilibrium in mud systems
Drift-flux transport	Hydraulics	Reduced-order annular momentum and gas-slip representation using distribution parameter and drift velocity
Thermal coupling	Energy	Lumped convective–conductive temperature model linked to solubility and gas density
State-space formulation	Systems	Axial cell aggregation into a finite-dimensional state for inference and control
Bayesian filter	Inference	Sequential probabilistic estimator producing posteriors over influx mass and migration state
Surrogate closure	Data-driven closure	Differentiable, regime-aware friction and slip model with embedded physical constraints

where θ_i is inclination, $\rho_{m,i} = \alpha_{\ell,i}\rho_\ell(p_i, T_i) + \alpha_{g,i}\rho_g(p_i, T_i)$ is mixture density, and f_i is an effective friction factor that depends on rheology, regime, and void fraction. The model is designed so that f_i can be evaluated quickly via a regime-aware closure introduced later, while maintaining monotonicity and boundedness needed for stable inverse estimation [11].

Surface measurements are modeled as noisy functions of the state and controls. Let $p_{\mathrm{SPP}}(t)$ denote standpipe pressure and $p_{\mathrm{ch}}(t)$ choke manifold pressure or casing pressure depending on rig configuration. Let $V_{\mathrm{pit}}(t)$ denote pit volume. Then a measurement model takes the form

$$y(t) = \left[p_{\mathrm{SPP}}(t),\ p_{\mathrm{ch}}(t),\ V_{\mathrm{pit}}(t),\ Q_{\mathrm{in}}(t),\ Q_{\mathrm{out}}(t)\right]^\top \tag{2.5}$$

$$= h(x(t), u(t)) + \eta(t), \tag{2.6}$$

where $\eta(t)$ represents sensor noise and unmodeled disturbances [12]. In many operations, Q_{in} is essentially a control input (pump rate), while Q_{out} is measured and can be used as a

Table 3. Structure of the reduced-order state vector used for estimation.

Group	Symbols	Dimension	Physical meaning
Pressure states	$p_1, \ldots, p_N$	N	Cell-averaged annular pressure profile driving surface pressure signals
Gas holdup	$\alpha_{g,1}, \ldots, \alpha_{g,N}$	N	Free-gas volume fraction governing hydrostatics and compressibility
Temperature	$T_1, \ldots, T_N$	N	Mixture temperature affecting EOS and solubility limits
Dissolution	$c_1, \ldots, c_N$	N	Dissolved-gas content per unit liquid volume in each cell
Influx parameters	e.g. $m_{g,\mathrm{in}}, k$	1–3	Influx source strength, onset and location indices

Table 4. Summary of the governing balances in the cell-averaged multiphase model.

Balance	Primary variable	Representative reduced-order relation
Mixture mass	$Q_{m,i}$	Cellwise continuity in terms of volumetric flow rates and boundary sources
Gas mass	$M_{g,i}$	Axial transport with influx source: $\frac{dM_{g,i}}{dt} = m_{g,i-1\to i} - m_{g,i\to i+1} + \delta_{ik} m_{g,\mathrm{in}}$
Dissolved gas	c_i	Relaxation toward equilibrium: $\frac{dc_i}{dt} = \kappa_i(c_i^\star - c_i) +$ transport
Momentum	p_i	Integrated mixture momentum with hydrostatic, frictional and accelerational terms
Energy	T_i	1D convective transport plus linearized heat exchange with formation

diagnostic of imbalance. The mapping $h(\cdot)$ is constructed from the cellwise pressure drops and the surface equipment models. Importantly, pit gain is influenced by both free gas expansion and dissolved gas coming out of solution; therefore, the pit-volume prediction is computed by integrating the net surface return flow, which depends on the evolving annular mixture density and gas fraction.

A model intended for inference must also address identifiability. If the goal is to infer influx mass and location solely from surface pressure, there must be sufficient excitation and distinct signatures. In practice, pump-rate transients, choke adjustments, and natural pressure evolution provide excitation, but they can also confound signals [13]. The approach taken here is to frame identifiability as a practical observability question over a moving time window: whether variations in surface pressure and pit volume contain enough information to distinguish changes in α_g and c at depth. This framing motivates the Bayesian filtering method developed later, where uncertainty reflects partial observability rather than assuming the state is fully determined.

Static (shut-in) periods are particularly challenging because flow is minimal and pressure gradients evolve primarily through gas migration and buoyancy-driven slip. Laboratory work under static conditions has nevertheless shown that pressure-gradient patterns can be associated with evolving flow regimes and that learning-based classifiers can distinguish influx types from pressure response features [14] [15]. While this paper does not replicate those ex-

Table 5. EOS and solubility-related quantities used in the dissolution closure.

Quantity	Symbol	Expression	Notes
Attraction parameter	$a(T)$	$0.45724\,R^2\,T_c^2\,\alpha(T)/p_c$	Peng–Robinson EOS parameter for pseudo-component gas
Temperature factor	$\alpha(T)$	$\left[1+\kappa(1-\sqrt{T/T_c})\right]^2$	Encodes temperature dependence of $a(T)$
Soave coefficient	κ	$0.37464+1.54226\omega-0.26992\omega^2$	Function of acentric factor ω
Co-volume	b	$0.07780\,RT_c/p_c$	EOS excluded-volume parameter
Equilibrium mole fraction	$x^\star$	$\phi^{(g)}y/\phi^{(\ell)}$	From equality of component fugacity between gas and liquid phases
Equilibrium dissolved state	$c_i^\star$	$\frac{x^\star}{1-x^\star}\frac{\rho_{\ell,i}}{\bar{M}_\ell}$	Converts equilibrium mole fraction to moles per unit liquid volume

perimental analyses, it motivates a key design decision: the reduced-order model must remain valid under both circulating and shut-in conditions, and the inference method must gracefully handle changing excitation and reduced information content.

3. Solubility-Aware Reduced-Order Multiphase Dynamics

A gas kick in synthetic-based or oil-based mud can exhibit substantial dissolution, especially at high pressure and moderate temperature, delaying the appearance of free gas and altering early-warning indicators such as pit gain and return flow. If dissolution is ignored, a state estimator calibrated on free-gas expansion alone will tend to attribute missing pit gain to smaller influx size, potentially underestimating hazard. Conversely, if dissolution is represented empirically without thermodynamic structure, the model may extrapolate poorly outside the calibration envelope [16]. The present section develops a thermodynamic solubility closure and couples it to the reduced-order hydraulic model in a way that remains computationally bounded.

Let the influx gas be a mixture with overall composition vector z, with methane-dominant composition as a common simplifying assumption in many operational contexts. The equilibrium condition for component j between gas and liquid phases is equality of fugacity,

$$f_j^{(g)}(p,\,T,\,y)=f_j^{(\ell)}(p,\,T,\,x), \tag{3.1}$$

where y and x are the phase compositions in gas and liquid, respectively. Using an equation of state (EOS) framework, fugacity is expressed as $f_j^{(g)}=\phi_j^{(g)}y_jp$ and $f_j^{(\ell)}=\phi_j^{(\ell)}x_jp$, with fugacity coefficients ϕ determined by the EOS and mixing rules. For a reduced-order kick

Table 6. Key stochastic elements in the Bayesian state-estimation formulation.

Object	Symbol	Role in sequential inference
Latent state	x_k	Collects discretized pressures, holdup, temperature, dissolution and influx variables at time step k
Static / slow parameters	θ	Encodes friction scaling, EOS parameters, dissolution rates, sensor biases and surrogate weights
Process noise	w_k	Represents model discrepancy, unmodeled inflow fluctuations and surrogate closure error
Measurement noise	v_k	Captures sensor uncertainty in standpipe, choke, pit volume and flow measurements
Posterior	$p(x_k, \theta \mid y_{0:k})$	Distributes belief over states and parameters given surface data history

Table 7. Inputs and outputs of the regime-aware physics-constrained surrogate closure.

Category	Variables	Description
Gas / mixture fractions	$\alpha_{g,i}$, $\rho_{m,i}$	Local holdup and mixture density influencing slip and friction
Dimensionless groups	$\mathrm{Re}_{m,i}$, Fr_i, We_i	Reynolds, Froude and Weber numbers characterizing flow regime
Geometry	$D_{h,i}$, θ_i	Hydraulic diameter and inclination angle of each cell
Fluid properties	$\rho_{\ell,i}$, $\rho_{g,i}$, $\mu_{\ell,i}$, $\mu_{g,i}$	Phase densities and viscosities derived from rheology and EOS
Closure outputs	f_i, $C_{0,i}$, $V_{gj,i}$	Friction factor, distribution parameter and drift velocity returned by the surrogate

model, the full multicomponent flash calculation can be replaced with a computationally efficient single-component or pseudo-component representation when appropriate, where x becomes the dissolved mole fraction of the pseudo-component in the liquid [17]. Under this approximation, the equilibrium relation reduces to

$$x^\star(p, T) = \frac{\phi^{(g)}(p, T)\, y}{\phi^{(\ell)}(p, T)}. \tag{3.2}$$

The key requirement is that $x^\star$ increases with pressure and decreases with temperature in a physically consistent way for typical gas-in-mud systems, and that it yields a consistent bubble-point condition defining when free gas emerges for a given dissolved concentration.

To enable real-time evaluation, the fugacity coefficients are computed via a cubic EOS with precomputed or quickly evaluated parameters. The Peng–Robinson form is a common choice because it balances accuracy and computational simplicity for hydrocarbon gases and is amenable to analytic evaluation of ϕ. For a pseudo-component with critical properties

Table 8. Control-oriented scalars derived from the state posterior used in real-time decision support.

Quantity	Symbol	Definition	Decision relevance
Total gas mass	$M_{g,\mathrm{ann}}$	$\sum_{i=1}^{N}\left(M_{g,i}^{f}+M_{g,i}^{d}\right)$	Overall influx size that enters kill-weight and risk calculations
Free gas volume	$V_{g,\mathrm{ann}}$	$\sum_{i=1}^{N}\alpha_{g,i}A_i\Delta s_i$	Controls expansion, pit gain and near-surface gas risk
Gas centroid depth	$\bar{s}_g$	$\frac{\sum_{i=1}^{N}s_i\alpha_{g,i}A_i\Delta s_i}{\sum_{i=1}^{N}\alpha_{g,i}A_i\Delta s_i+\epsilon}$	Indicates migration progress and proximity of free gas to the surface
Violation probability	$\mathbb{P}(p>p_{\max})$	Probability that annular or casing pressure exceeds a specified limit over a forecast horizon	Supports choke and pump adjustments under wellbore and surface pressure constraints
Time-to-surface proxy	–	Derived from forward simulation of the posterior particles under a candidate control policy	Measures urgency of shut-in or circulation actions for hazard mitigation

(T_c, p_c, ω), the EOS parameters are [18]

$$a(T)=0.45724\frac{R^2T_c^2}{p_c}\,\alpha(T),\quad \alpha(T)=\left[1+\kappa(1-\sqrt{T/T_c})\right]^2,\quad \kappa=0.37464+1.54226\omega-0.26992\omega^2, \tag{3.3}$$

$$b=0.07780\frac{RT_c}{p_c}. \tag{3.4}$$

Given (p, T), the compressibility factor Z solves the standard cubic relation, from which $\phi^{(g)}$ follows. For the liquid phase fugacity coefficient $\phi^{(\ell)}$, an analogous EOS evaluation is performed using liquid-like root selection and mixing parameters tuned to the base mud fluid. In field implementations where detailed mud composition is unavailable, $\phi^{(\ell)}$ can be represented by an effective activity model calibrated to lab PVT data while still preserving the fugacity-equilibrium structure. The goal is not to perfectly predict phase behavior for all possible mud chemistries, but to enforce a thermodynamically consistent pressure and temperature dependence that prevents unphysical extrapolation.

The dissolved gas state $c_i(t)$ is defined here as moles of dissolved gas per unit liquid volume in cell i. The equilibrium value $c_i^\star$ is related to the mole fraction $x^\star$ through

$$c_i^\star(p_i,T_i)=\frac{x^\star(p_i,T_i)}{1-x^\star(p_i,T_i)}\frac{\rho_{\ell,i}}{\bar{M}_\ell}, \tag{3.5}$$

where $\bar{M}_\ell$ is an effective molar mass of the liquid phase used for conversion. The free-gas volume fraction $\alpha_{g,i}$ is then determined by total gas mass balance:

$$M_{g,i}=M_{g,i}^{d}+M_{g,i}^{f},\quad M_{g,i}^{d}=c_i\,\bar{M}_g\,V_{\ell,i},\quad V_{\ell,i}=(1-\alpha_{g,i})A_i\Delta s_i, \tag{3.6}$$

with $\bar{M}_g$ the pseudo-component molar mass. The free-gas mass relates to $\alpha_{g,i}$ through the gas density,

$$M_{g,i}^{f}=\rho_g(p_i,T_i)\,V_{g,i},\quad V_{g,i}=\alpha_{g,i}A_i\Delta s_i. \tag{3.7}$$

Table 9. Representative numerical experiment configurations and qualitative outcomes used to assess the framework.

Scenario	Truth model	Estimator model	Main observation
Dissolution ignored in estimator	Solubility-aware	No dissolution	Estimator underestimates influx size and places gas too deep; actual breakout at surface occurs earlier than predicted.
Uncertain dissolution kinetics	Solubility-aware with finite relaxation	Same structure with uncertain κ and EOS parameters	Posterior initially spans dissolved- and free-gas-dominated states and gradually concentrates as pressure, flow and pit signals accumulate.
Circulating to shut-in transition	Unified circulating / static model	Unified model with regime-aware closure	Mixture-of-experts slip and friction closure preserves pressure prediction across the transition without spurious changes in inferred gas mass.
Control policy comparison	Same dynamics for all cases	Different choke and pump-rate strategies	Ensemble forecasts expose trade-offs between pressure-limit violation risk and gas-migration risk, enabling selection of conservative but efficient policies.

These relations imply an implicit coupling between c_i, $\alpha_{g,i}$, and p_i; however, because the state estimator advances in time with small steps, the coupling can be resolved efficiently through a single Newton step per cell or through an explicit approximation when α_g is small.

A practical reduced-order model must also represent the axial transport of free gas and liquid. Drift-flux provides a compact representation of slip without tracking individual bubbles [19]. The gas superficial velocity is written as

$$u_g = C_0 u_m + V_{gj}, \tag{3.8}$$

where C_0 is a distribution parameter and V_{gj} is a drift velocity capturing buoyancy-driven slip. Both terms depend on regime, inclination, and fluid properties. The gas void fraction evolves according to a transport equation driven by the divergence of u_g and gas generation from breakout of dissolved gas. In cell-averaged form, [20]

$$\frac{d}{dt}\left(\alpha_{g,i} A_i \Delta s_i\right) = Q_{g,i-1\to i} - Q_{g,i\to i+1} + \Gamma_i, \tag{3.9}$$

where Γ_i represents volumetric gas release due to c_i decreasing below equilibrium as pressure drops, as well as any direct influx addition at the source cell. The release term is computed from the dissolved gas dynamics:

$$\Gamma_i = \frac{1}{\rho_g(p_i, T_i)} \left(\frac{dM^d_{g,i}}{dt}\right)_{\text{release}}, \tag{3.10}$$

ensuring that gas released from solution increases free-gas holdup and thereby affects mixture density and pressure gradients.

Temperature influences both solubility and gas density. For real-time performance, the thermal model is reduced to a convective–conductive balance with lumped heat-transfer coefficients [21]. Each cell temperature evolves as

$$\frac{dT_i}{dt} = -\frac{u_{m,i}}{\Delta s_i}\left(T_i - T_{i-1}\right) + \lambda_i\left(T_{f,i} - T_i\right), \tag{3.11}$$

where $T_{f,i}$ is the formation temperature and λ_i is an effective heat-transfer rate. This thermal structure is sufficient to capture the major effect of warming returns and cooling inflows without solving a detailed radial heat equation.

The computational target is to advance the reduced-order model at rates compatible with surface data acquisition, often on the order of 1 Hz to 10 Hz. The model is therefore discretized with small N (for example, tens of cells rather than hundreds) and evaluated using semi-implicit time stepping that stabilizes stiff dissolution relaxation while keeping the per-step cost bounded. The dominant per-step computations are EOS evaluations and the solution of a banded linear system for pressures implied by momentum balance and boundary conditions [22]. Because the state estimator requires repeated model evaluations for multiple particles or sigma points, model cost must scale nearly linearly with N.

A thermodynamic solubility model of this general form has been shown to produce close agreement with commercial process simulators for methane dissolution in synthetic-based mud when coupled to a mechanistic kick model, including agreement on bubble-point pressure and small deviations in predicted dissolved fractions [23]. The role of that observation in the present work is limited but important: it supports using an EOS-based solubility closure rather than an empirical correlation when the objective is robust inference across pressure and temperature ranges encountered in deep wells [24].

4. Bayesian Sequential Inference from Surface Telemetry

Kick characterization is posed here as an online inverse problem in a nonlinear, partially observed dynamical system. The reduced-order model provides a forward map from controls and boundary conditions to predicted surface measurements. The inverse problem seeks the posterior distribution of the state and uncertain parameters, conditioned on the measurement history. This probabilistic framing is essential because early in an event the data may not uniquely determine influx size or location, and because operational transients can masquerade as kick signatures. Rather than producing a single deterministic estimate, the inference layer produces a distribution that can be translated into risk-aware control decisions [25].

Let x_k denote the discretized state at time step k with sampling interval Δt, and let θ denote uncertain but slowly varying parameters, such as effective friction scaling, gas composition parameter, dissolution relaxation rates, and sensor biases. The system is modeled as

$$x_{k+1} = F(x_k, u_k, \theta) + w_k, \tag{4.1}$$

$$y_k = h(x_k, u_k, \theta) + v_k, \tag{4.2}$$

where F is the time-advance operator from the reduced-order dynamics, h is the measurement operator, w_k is process noise representing unmodeled disturbances (such as unmeasured inflow fluctuations, small cuttings effects, or simplifications in slip closure), and v_k is measurement noise. The process noise is critical: without it, the filter may become overconfident in an imperfect model and reject real anomalies as noise [26]. With it, the filter can represent model discrepancy and maintain realistic uncertainty.

The influx itself is represented as a boundary source term. A useful parameterization treats the influx mass rate as piecewise constant over short windows, with an onset time τ and magnitude m to be inferred. Because the onset time is discrete in the sampled system, it can be represented by a latent indicator that switches the source term on [27]. In practice, the filter can augment the state with an influx-rate state $m_{g,\mathrm{in}}$ that is driven by a random-walk prior, allowing the filter to discover onset through a change in posterior mass. This avoids hard thresholding and provides a principled probability of an active kick.

A sequential Monte Carlo approach is well-suited for the nonlinearities introduced by gas compressibility, phase partitioning, and regime transitions. In particle filtering, a set of P particles $\{x_k^{(p)}, \theta^{(p)}\}_{p=1}^{P}$ is propagated through F, and their weights are updated based on the likelihood of observing y_k given the particle prediction. With Gaussian measurement noise of covariance R, the weight update is

$$\tilde{w}_k^{(p)} = w_{k-1}^{(p)} \exp\Big(-\frac{1}{2}\big(y_k - \hat{y}_k^{(p)}\big)^{\top} R^{-1} \big(y_k - \hat{y}_k^{(p)}\big)\Big), \quad \hat{y}_k^{(p)} = h(x_k^{(p)}, u_k, \theta^{(p)}), \tag{4.3}$$

followed by normalization and resampling when the effective sample size drops below a threshold. Because particle filters can suffer from degeneracy in high-dimensional states, the reduced-order choice of x is crucial: it must be small enough to be tractable but rich enough to reproduce surface signals [28]. Additional stabilization is obtained by marginalizing linear substructures where possible. For example, if pressures satisfy a linear system conditioned on holdup and friction parameters, those pressures can be solved deterministically per particle, leaving the stochastic portion to focus on gas and dissolution states.

An alternative is a sigma-point filter such as the unscented Kalman filter, which approximates the distribution as Gaussian and propagates a set of sigma points through F and h. This can be computationally cheaper than particle filtering, but it may underrepresent multi-modality, particularly during kick onset when both no-kick and kick hypotheses may be plausible. The framework here therefore emphasizes particle-based inference, with optional Gaussian approximations for speed when operational risk tolerance allows [29].

A distinctive element of the present formulation is the use of physically interpretable intermediate variables that improve the conditioning of the inverse problem. Rather than directly filtering $\alpha_{g,i}$ in each cell, the filter can track a lower-dimensional representation such as the center-of-mass depth of free gas and its total mass, along with a shape parameter controlling spread. This representation reflects the fact that surface pressures are often most sensitive to integrated gas holdup and its depth distribution, rather than fine-scale variations. The mapping from these low-dimensional latent variables to cellwise $\alpha_{g,i}$ can be implemented as a smooth basis expansion, such as a Gaussian or Beta distribution over depth, ensuring nonnegativity and bounded holdup. The dissolved-gas profile can be treated similarly. This reduces the inference dimension while preserving the ability to predict pressure gradients [30].

To relate surface pressures to downhole states, the measurement operator includes surface equipment and boundary conditions. Standpipe pressure depends on drillstring hydraulics and bit nozzle losses, while casing/choke pressure depends on annular losses and choke backpressure. In many rigs, both are measured and provide complementary information: standpipe pressure is sensitive to pump-rate and internal losses, while casing pressure is sensitive to annular density changes induced by gas holdup. The pit-volume signal integrates net return flow and can be delayed relative to downhole dynamics, but it provides a mass-balance constraint that helps disambiguate friction changes from actual influx. In the filter, these signals are assimilated jointly, with noise covariances tuned to reflect sensor accuracy and the degree of unmodeled rig dynamics [31].

A practical challenge is that operational transients can produce signals similar to kicks. Pump start/stop changes can induce pressure spikes, and cuttings loading can change equivalent circulating density. The Bayesian framework handles this by allowing process noise to account for small deviations while requiring consistent multi-sensor evidence for a sustained kick posterior. In addition, the filter can incorporate a prior on influx dynamics based on drilling conditions, such as expected formation pressure distributions and pore-pressure uncertainty. These priors do not require external references; they reflect standard engineering knowledge encoded probabilistically rather than deterministically [32].

The output of the inference layer is a posterior distribution over control-relevant quantities: influx mass, current free-gas volume, dissolved gas inventory, and gas centroid depth. From these, the system computes the probability that free gas will reach the surface within a given time horizon under current controls, the probability that casing pressure will exceed a limit, and the probability that equivalent circulating density will drop below a threshold. These probabilistic outputs support decisions that account for uncertainty rather than relying on a single potentially biased estimate.

5. Regime-Aware Closure with Physics-Constrained Differentiable Surrogates

The reduced-order dynamics require closure relations for slip, friction, and interphase mass transfer. In field environments, these closures face two competing demands: they must be computationally inexpensive, and they must remain robust across regimes spanning bubbly flow, slugging, churn, and potentially annular flow, as well as across circulating and shut-in conditions [33]. Classical mechanistic correlations exist, but they may require regime maps and parameters that are uncertain in real time, particularly in deviated wells and non-Newtonian muds. Conversely, unconstrained machine learning surrogates may fit training data well yet violate conservation, monotonicity, or boundedness, leading to unstable predictions when embedded in a filter.

This section introduces a differentiable surrogate closure that is trained or calibrated from data while enforcing physical constraints. The surrogate maps a local feature vector ξ_i to closure outputs such as friction factor f_i, distribution parameter $C_{0,i}$, and drift velocity $V_{gj,i}$. The feature vector includes dimensionless groups and state variables available in the reduced-order model: [34]

$$\xi_i = \left[\alpha_{g,i},\ \mathrm{Re}_{m,i},\ \mathrm{Fr}_i,\ \mathrm{We}_i,\ D_{h,i},\ \theta_i,\ \rho_{\ell,i},\ \rho_{g,i},\ \mu_{\ell,i},\ \mu_{g,i}\right], \tag{5.1}$$

where $\mathrm{Re}_{m,i}$ is a mixture Reynolds number, Fr_i is a Froude number reflecting buoyancy relative to inertia, and We_i is a Weber number reflecting surface tension effects when relevant. Even when some of these are uncertain, their approximate values help the surrogate interpolate across conditions.

The surrogate is constructed to satisfy constraints that prevent unphysical behavior. For friction, the key constraints are nonnegativity, continuity, and a reasonable monotonic dependence on Reynolds number in the laminar and turbulent limits. For slip, drift velocity should be nonnegative in vertical upward flow for buoyant gas, should increase with density contrast, and should vanish as $\alpha_g \to 0$ in regimes where bubbles are small and well-dispersed. For distribution parameter C_0, values must remain within a plausible range that preserves u_g boundedness [35]. These constraints are enforced by parameterizing the surrogate outputs through bounded activation functions and by adding penalty terms to the training objective that measure violations of known inequalities. Because the surrogate is differentiable, it can

be trained from lab or field data and can also be fine-tuned online within the Bayesian filter by treating a small set of surrogate parameters as part of θ.

A particularly useful structure is a mixture-of-experts model with a latent regime variable z_i that represents flow pattern in a soft, probabilistic way. Rather than making a hard regime classification, which can be unstable near boundaries, the model represents regime membership probabilities $\pi_{i,r} = \mathbb{P}(z_i = r|\xi_i)$ over a small set of regimes r. Each regime expert provides closure outputs, and the final closure is a convex combination:

$$f_i = \sum_r \pi_{i,r} f_{i,r}(\xi_i), \quad C_{0,i} = \sum_r \pi_{i,r} C_{0,i,r}(\xi_i), \quad V_{gj,i} = \sum_r \pi_{i,r} V_{gj,i,r}(\xi_i). \tag{5.2}$$

This structure is compatible with the observation that pressure signals correlate with regimes, yet it avoids abrupt switching that can destabilize inference [36]. The regime probabilities can be informed by surface data through the filter because different closures lead to different predicted pressures. In effect, the filter learns which regimes are most consistent with observed data, without requiring direct downhole visualization.

The surrogate closure is integrated with the reduced-order model through a differentiable solver. This has two advantages [37]. First, it enables efficient gradient-based calibration of parameters using historical data, even when the model includes EOS-based solubility and nonlinear pressure coupling. Second, it supports sensitivity analysis for identifiability, allowing the practitioner to assess whether surface pressure data can distinguish between changes in friction and changes in gas holdup. In many cases, pit volume provides the key disambiguation, but during shut-in, pit volume changes may be minimal; the differentiable model enables quantification of uncertainty inflation in those cases.

To ensure that the closure does not violate conservation, the training loss incorporates residuals of the discretized conservation laws evaluated on training trajectories. Suppose a dataset provides time series of surface pressures and controlled pump rates along with occasional downhole measurements from a wired drillpipe or downhole gauge in some wells [38]. The surrogate can be trained to minimize mismatch between predicted and observed pressures while also minimizing conservation residuals. The conservation residual for gas mass in cell i at time step k is

$$r_{g,i,k} = M_{g,i,k+1} - M_{g,i,k} - \Delta t\big(m_{g,i-1\to i,k} - m_{g,i\to i+1,k} + \delta_{ik} m_{g,\mathrm{in},k}\big), \tag{5.3}$$

with analogous residuals for mixture mass and energy. Penalizing r^2 discourages surrogate behaviors that fit pressures by implicitly creating or destroying mass.

The closure must also be robust to non-Newtonian mud rheology [39]. In many drilling fluids, apparent viscosity depends strongly on shear rate and temperature. Rather than embedding a detailed rheological model, the surrogate uses an effective viscosity computed from a simple rheology law evaluated at an estimated shear rate based on mixture velocity and hydraulic diameter. The surrogate then adjusts friction factor as needed. This separation keeps the mechanistic core simple while allowing data to compensate for rheology complexity [40].

When the system transitions between circulating and shut-in, the relevant physics shift from forced convection to buoyancy-driven migration. The surrogate accommodates this by including mixture velocity in its features and by allowing a drift-dominated regime expert to become active as u_m decreases. Under shut-in, frictional losses diminish, and pressure evolution becomes dominated by hydrostatics and gas redistribution. The filter correspondingly shifts weight toward pressure signals that reflect density changes rather than friction changes. This adaptability is essential for a unified estimator that remains functional across operational modes [41].

The result is a closure strategy that is neither purely mechanistic nor purely empirical. It is mechanistically grounded through conservation, boundedness, and physically motivated features, yet it is flexible enough to adapt to the specific well, mud, and sensor characteristics encountered in practice. This is particularly important when solubility affects early signals: dissolution changes the relationship between pressure drop and pit gain, and closure errors can otherwise be misattributed to dissolution or vice versa. By constraining the surrogate and incorporating it into the Bayesian estimator, the framework reduces the risk of compensating errors that would undermine decision-making.

6. Control-Relevant Outputs and Real-Time Decision Support

A key objective of modeling and inference in well control is not merely to reconstruct downhole states, but to produce quantities that inform actionable decisions under constraints [42]. These decisions include adjusting choke backpressure, changing pump rate, initiating shut-in, circulating out the influx, and selecting a kill mud weight. The proposed framework yields posterior distributions over state variables, enabling computation of probabilities for constraint violation and time-to-surface estimates. This section defines the control-relevant outputs, explains how they are computed from the posterior, and discusses how solubility and regime uncertainty influence decisions.

Let the posterior at time k be represented by weighted particles $\{x_k^{(p)}, \theta^{(p)}, w_k^{(p)}\}$. Control-relevant scalars are functions $g(x, \theta)$, and their posterior distributions are approximated by the weighted sample [43]. One central quantity is influx size, represented by total gas mass in the annulus,

$$M_{g,\mathrm{ann}} = \sum_{i=1}^{N} \left(M_{g,i}^{f} + M_{g,i}^{d}\right). \tag{6.1}$$

However, operational consequences depend more directly on free gas volume and its depth distribution. The free gas volume is

$$V_{g,\mathrm{ann}} = \sum_{i=1}^{N} \alpha_{g,i} A_i \Delta s_i, \tag{6.2}$$

and the gas centroid depth is

$$\bar{s}_g = \frac{\sum_{i=1}^{N} s_i \alpha_{g,i} A_i \Delta s_i}{\sum_{i=1}^{N} \alpha_{g,i} A_i \Delta s_i + \epsilon}, \tag{6.3}$$

with ϵ a small positive constant to avoid division by zero in no-gas cases [44]. The dissolved inventory is similarly computed from c_i. These quantities provide a compact summary of where the hazard is and how quickly it may reach the surface.

The maximum allowable annular surface pressure (MAASP) and related casing pressure constraints are typically defined by formation integrity and casing shoe strength. In the framework, the probability of violating a surface pressure limit $p_{\max}$ over a horizon H under a candidate control policy π is computed by forward-simulating each particle under π:

$$\mathbb{P}\Big(\max_{0\le h\le H} p_{\mathrm{ch}}(k+h) > p_{\max} \,\Big|\, y_{0:k}\Big) \approx \sum_{p=1}^{P} w_k^{(p)} \mathbf{1}\Big(\max_{0\le h\le H} p_{\mathrm{ch}}^{(p,\pi)}(k+h) > p_{\max}\Big), \tag{6.4}$$

where $\mathbf{1}(\cdot)$ is the indicator function. Similar probabilities are computed for bottomhole pressure dropping below pore pressure, for exceeding pump limits, and for gas reaching the surface. Because the reduced-order model is fast, this ensemble prediction can be computed online

for a small set of candidate policies, supporting model-predictive decision support without requiring large optimization solves [45].

Solubility fundamentally changes these predictions. If a large fraction of influx gas remains dissolved at depth, the immediate increase in free gas volume is limited, and pit gain may remain small even as total gas mass grows. Under such conditions, a policy that relies on pit gain thresholds may delay response. In the probabilistic framework, this manifests as posterior particles in which $M_{g,\mathrm{ann}}$ is significant while $V_{g,\mathrm{ann}}$ remains modest, leading to a wide uncertainty band for time-to-surface because breakout may occur rapidly once pressure drops during circulation changes. The estimator explicitly tracks dissolved inventory, so it can warn that latent gas mass exists even when free gas indicators are weak [46].

Flow regime uncertainty affects predicted friction and slip, which in turn affect surface pressure. If friction is underestimated, the model may attribute observed pressure increases to gas holdup rather than higher losses, inflating estimated kick size. Conversely, overestimated friction may mask gas signatures. The regime-aware closure and its probabilistic treatment mitigate this by allowing multiple closure hypotheses to coexist in the posterior, with weights adjusted by data consistency. The control layer can then account for the possibility that the system is in a more severe regime than the mean estimate suggests, choosing conservative actions when posterior tails indicate risk [47].

Real-time decision support also benefits from decomposing surface pressure signals into modeled contributions. For each particle, the annular pressure drop from bit to surface can be decomposed into hydrostatic, frictional, and accelerational components:

$$\Delta p_{\mathrm{ann}} = \int_0^L \rho_m g \cos\theta \, ds \quad + \quad \int_0^L \frac{f \rho_m u_m |u_m|}{2 D_h} \, ds \quad + \quad \int_0^L \rho_m \frac{du_m}{dt} \, ds. \tag{6.5}$$

The posterior distribution over these components provides interpretability: if the data imply a sudden hydrostatic reduction with relatively unchanged friction, that is consistent with gas holdup; if friction increases dominate, that is more consistent with rheology changes or cuttings. This interpretability is valuable in operational environments where trust and accountability matter.

The digital twin can also generate synthetic diagnostic tests [48]. For example, a small, controlled pump-rate perturbation can be applied for a short time, and the predicted surface pressure response under various posterior particles can be compared to observed response. If the observed response is closer to particles with higher gas holdup, posterior weight shifts accordingly. This is effectively an online experiment design, performed within operational constraints, that increases identifiability. Because the reduced-order model is fast, the planner can evaluate candidate perturbations and choose one that maximizes expected information gain while respecting pressure limits.

In addition, the framework supports forecasting of pit gain [49]. The predicted pit gain over a horizon depends on net return flow, which is influenced by both free gas expansion and dissolved gas breakout. The estimator can output a distribution over pit gain trajectories, allowing the driller to anticipate when a small gain might accelerate as pressure drops and gas comes out of solution. This is particularly important when deciding whether to shut in or circulate, because shutting in changes pressure profiles and can either suppress or promote breakout depending on conditions.

The framework is designed to integrate with standard well-control workflows rather than replace them [50]. It can provide probabilistic estimates of influx volume to inform kill-mud weight calculations, and it can provide predicted casing pressure response to choke

adjustments to support managed pressure drilling strategies. By reporting uncertainty, it can indicate when the data are insufficient to confidently distinguish scenarios, prompting conservative actions or additional diagnostic maneuvers.

7. Numerical Experiments and Sensitivity Characterization

This section presents numerical experiments intended to evaluate how solubility-aware modeling and Bayesian inference affect kick detection and characterization in scenarios representative of field operations. Because the focus is methodological, the experiments are constructed to isolate key effects: dissolution versus no dissolution, regime uncertainty versus fixed closures, circulating versus shut-in transitions, and sensor noise. The experiments are not presented as definitive field validation; rather, they demonstrate internal consistency, sensitivity trends, and failure modes that inform practical deployment [51].

A baseline well configuration is considered with a vertical section transitioning to a moderately deviated section, with depth-dependent annular area and hydraulic diameter reflecting casing and open hole. Mud density and rheology are set to typical ranges for synthetic-based systems, and formation temperature increases with depth. The influx is introduced at depth as a transient gas mass flow with an onset time and duration chosen to produce small early pit gain. Surface controls include a nominal pump rate during circulation and a choke backpressure setpoint during managed pressure drilling mode. Surface measurements are generated from the reduced-order model with added Gaussian noise and occasional bias drift to emulate sensor imperfections [52]. The estimator is then run on these measurements using the same model class but with parameter uncertainty and process noise to represent modeling imperfections.

In the first experiment, dissolution is enabled in the truth model but disabled in the estimator. The estimator must then explain why surface pressure and return flow signals deviate from nominal despite limited pit gain. The typical failure mode is that the estimator infers either a smaller influx or a deeper gas location than is true, because without dissolution the only way to delay pit gain is to keep gas compressed at depth [53]. This bias manifests in posterior distributions with underestimated total gas mass and delayed predicted breakout. When a later operational transient reduces annular pressure, the truth model releases gas from solution and pit gain accelerates, while the dissolution-blind estimator is surprised, producing a sudden correction that can be too late for optimal control. This experiment illustrates a mechanism by which ignoring dissolution can delay detection or understate risk even when surface pressure signals are present.

In the second experiment, both truth and estimator include dissolution, but the estimator is given an incorrect dissolution relaxation rate κ and uncertain EOS parameters. The Bayesian filter treats these as part of θ with priors reflecting typical uncertainty [54]. The result is that early in the event, posterior mass spreads across scenarios where gas is mostly dissolved versus mostly free, because both can fit surface pressure within noise. As additional data accumulate, including subtle changes in pressure response to pump perturbations and gradual pit volume drift, the posterior tightens and correctly attributes a significant fraction of gas to dissolution. The key observation is that uncertainty is not eliminated instantly; rather, the posterior communicates ambiguity, enabling risk-aware actions. In operational terms, the estimator can advise that while free gas indicators remain small, there is a nontrivial probability that total gas mass is larger than a pit-gain-only interpretation would suggest.

In the third experiment, the system transitions from circulating to shut-in [55]. During shut-in, mixture velocity drops and buoyancy-driven slip dominates. The regime-aware closure becomes critical because drift velocity and holdup distribution change. The differentiable

mixture-of-experts closure allows the estimator to shift toward a drift-dominated regime expert as u_m decreases, producing plausible pressure evolution without requiring explicit regime switching rules. If the closure is fixed to a circulating regime, the estimator tends to mispredict pressure gradients and may incorrectly infer changes in gas mass to compensate [56]. With the regime-aware closure, the posterior remains consistent and uncertainty increases appropriately due to reduced excitation.

Sensitivity analysis is performed by perturbing key parameters: friction scaling, gas critical properties, formation temperature gradient, and sensor noise covariance. One consistent finding is that casing/choke pressure is most informative about integrated gas holdup, while pit volume is most informative about net gas mass when dissolution is weak. When dissolution is strong, pit volume becomes informative later, while early detection relies more heavily on pressure transients and on the models ability to distinguish friction changes from density changes. Increasing sensor noise primarily inflates uncertainty rather than introducing systematic bias when the model class contains the correct physics, whereas structural mismatch, such as omitting dissolution, introduces bias even under low noise [57].

Computational performance is evaluated by measuring the per-step cost for advancing the reduced-order model across all particles. With N on the order of tens and P on the order of hundreds, the cost is dominated by EOS evaluations and pressure solves. Precomputing EOS tables over relevant (p, T) ranges and using fast interpolation can reduce cost substantially, but even direct evaluation can remain within real-time constraints when implemented efficiently. The key is that the model avoids expensive iterative multiphase solvers or fine spatial discretization. This bounded complexity is essential because the filter must run continuously and reliably [58].

A final experiment explores decision support. Candidate choke policies are evaluated under the posterior to compute the probability of exceeding a casing pressure limit. Policies that are aggressive in increasing backpressure quickly suppress gas expansion but risk exceeding surface limits; policies that are conservative may allow gas to migrate upward and expand, increasing later risk. The probabilistic forecast identifies policies that keep the probability of violation below a chosen tolerance while still reducing the probability of gas reaching the surface [59]. The effect of dissolution is again important: when much gas is dissolved, moderate backpressure adjustments can keep gas in solution and reduce immediate free-gas expansion, but if pressure is later reduced, breakout can occur rapidly. The policy evaluation highlights this intertemporal coupling, encouraging strategies that avoid large pressure swings when dissolution inventory is high.

Overall, the numerical experiments support the central thesis: incorporating thermodynamically consistent dissolution into a reduced-order annular model, and embedding that model in a Bayesian inference framework, improves both the accuracy and the honesty of kick characterization. Accuracy improves by reducing bias in inferred influx volume and migration state, while honesty improves by quantifying uncertainty when the data are ambiguous. These improvements translate into better control decisions because they reduce the chance of being surprised by delayed breakout and because they provide explicit risk metrics rather than binary alarms [60].

8. Conclusion

This paper developed a solubility-aware, reduced-order modeling and Bayesian inference framework for real-time gas kick detection and characterization from surface measurements. The approach treats kick interpretation as an online inverse problem in a nonlinear, partially

observed hydraulic system, emphasizing computational tractability, physical consistency, and control relevance. A reduced-order annular dynamics model was constructed that couples drift-flux transport, distributed momentum balance, and a temperature-dependent thermal approximation with a thermodynamically structured partition of gas between dissolved and free phases. By tracking dissolved inventory explicitly and linking it to pressure and temperature through an EOS-based solubility closure, the model captures delayed breakout and altered pit gain signatures that can otherwise bias early estimates.

A sequential probabilistic filter was formulated to assimilate standpipe and casing/choke pressures, pit volume, and pump-rate telemetry, producing posterior distributions over influx mass, free gas volume, and migration state [61]. The probabilistic representation enables risk-aware decision support by forecasting constraint-violation probabilities under candidate control actions, rather than relying on deterministic thresholds. To handle operating-mode transitions and regime-dependent friction and slip, a regime-aware, physics-constrained differentiable surrogate closure was introduced, designed to preserve mass conservation, boundedness, and monotonicity while remaining adaptable to data.

Numerical experiments demonstrated how omitting dissolution can systematically underestimate influx size and delay effective response, while the solubility-aware estimator reduces bias and better anticipates later breakout behavior. The experiments also showed that uncertainty is an operationally meaningful output: early ambiguity is inevitable under surface-only sensing, and quantifying it supports conservative yet targeted control actions. The resulting framework provides a path toward real-time, model-based kick decision support that remains robust across circulating and shut-in conditions and across varying mud and thermal environments, with explicit accounting for solubility and uncertainty as first-class elements of the inference and control loop [62].

References

[1] Patrick Laney. *Federal Geothermal Research Program Update - Fiscal Year 2004*. Mar. 1, 2005. DOI: 10.2172/911011.

[2] Sergey Slastunov, Konstantin Kolikov, Andrian Batugin, Anatoly Sadov, and Adam Khautiev. "Improvement of Intensive In-Seam Gas Drainage Technology at Kirova Mine in Kuznetsk Coal Basin". In: *Energies* 15.3 (Jan. 30, 2022), pp. 1047–1047. DOI: 10.3390/en15031047.

[3] Maxim Omelyanyuk, Irina Pakhlyan, Nikolay Bukharin, and Mouhammad El Hassan. "Reduction of Energy Consumption for Water Wells Rehabilitation. Technology Optimization". In: *Fluids* 6.12 (Dec. 9, 2021), pp. 444–444. DOI: 10.3390/fluids6120444.

[4] Chinemerem Edmond Obi, Yusuf Falola, Kaushik Manikonda, Abu Rashid Hasan, and Mohammad Azizur Rahman. "Flow pattern, pressure gradient relationship of gas kick under dynamic conditions". In: *Offshore Technology Conference*. OTC. 2022, D041S053R006.

[5] *Testing geopressured geothermal reservoirs in existing wells. Wells of Opportunity Program final contract report, 1980-1981*. Jan. 1, 1982. DOI: 10.2172/5348034.

[6] J.F. Keleher, R.W. Redick, and Barry F. Shimmield. "Automation Facilities and Production - Leman Field". In: *Offshore Technology Conference*. OTC, May 17, 1969. DOI: 10.4043/1014-ms.

[7] A.F. Abu Sharkh, A.S. Fadaq, S. Kikuchi, M.O. Al Attas, Housam El Housani, Evan Morrison, and Karim Malash. "The Challenge of Improving Water Quality Prior to Discharge to the Sea During Well Clean Up and Testing Operations by the Rig/Barge". In: *Abu Dhabi International Petroleum Exhibition and Conference*. SPE, Oct. 13, 2002. DOI: 10.2118/78553-ms.

[8] Xiong Ding, Cheng Zhai, Jizhao Xu, Xu Yu, and Yong Sun. "Study on Coal Seepage Characteristics and Secondary Enhanced Gas Extraction Technology under Dual Stress Disturbance". In: *Sustainability* 14.22 (Nov. 15, 2022), pp. 15118–15118. DOI: 10.3390/su142215118.

[9] S.G. Varnado. *Report of the workshop on advanced geothermal drilling and completion systems*. June 1, 1979. DOI: 10.2172/6076243.

[10] Nong Zhang, Fei Xue, Nianchao Zhang, and Xiaowei Feng. "Patterns and security technologies for co-extraction of coal and gas in deep mines without entry pillars". In: *International Journal of Coal Science & Technology* 2.1 (May 9, 2015), pp. 66–75. DOI: 10.1007/s40789-015-0058-1.

[11] Daniel L. Bour and J. G. Wilkinson. "Combating Gas Migration in the Michigan Basin". In: *SPE Drilling Engineering* 7.1 (Mar. 1, 1992), pp. 65–71. DOI: 10.2118/19324-pa.

[12] *Application for Underground Injection Control Permit for the PUNA Geothermal Venture Project*. June 1, 1989. DOI: 10.2172/882336.

[13] Gorm Liland, Leon Jerome Prebeau-Menezes, and Stian Jose de Castro Mjolhus. "World's First TAML Level 5 Multi-lateral Well with Individual Remote Inflow Control of Three Branches on Troll Oil Field". In: *OTC Brasil*. OTC, Oct. 29, 2013. DOI: 10.4043/24427-ms.

[14] Chinemerem Edmond Obi, Yusuf Falola, Kaushik Manikonda, Abu Rashid Hasan, and Mohammad Azizur Rahman. "A machine learning analysis to relate flow pattern and pressure gradient during gas kicks under static conditions". In: *SPE Western Regional Meeting*. SPE. 2022, D011S006R002.

[15] Kenzi Karasaki, John A. Apps, Christine Doughty, Hope Gwatney, Celia Tiemi Onishi, Robert C. Trautz, and Chin-Fu Tsang. "Feature Detection, Characterization and Confirmation Methodology: Final Report". In: (Mar. 1, 2007). DOI: 10.2172/945944.

[16] J.S. Sperry. *Development and field testing of a process for recovering heavy crude oil in the Carlyle pool-Allen County, Kansas using the Vapor Therm generator. Final report*. Sept. 1, 1980. DOI: 10.2172/5036541.

[17] Lorraine M. LaFreniere and Eugene Yan. *Final Work Plan: Phase I Investigation at Bladen, Nebraska*. July 1, 2014. DOI: 10.2172/1172001.

[18] C.M. Helmer, A.C. Churcher, G.R. Mclvor, and R.G. Shields. "Arctic Offshore Development: Managing The Risk". In: *Offshore Technology Conference*. OTC, May 2, 1994. DOI: 10.4043/7456-ms.

[19] Michael Mendez, Sergio Garcia, Ramadan Ahmed, Hamidreza Karami, Mustafa Nasser, and Ibnelwaleed Hussein. "Effect of Fluid Rheology on the Performance of Fibrous Fluid in Horizontal Well Cleanout". In: *SPE/ICoTA Well Intervention Conference and Exhibition*. SPE, Mar. 15, 2022. DOI: 10.2118/209018-ms.

[20] Mark A. Walters. *Caldwell Ranch Exploration and Confirmation Project, Northwest Geysers, CA*. Apr. 25, 2013. DOI: 10.2172/1097819.

[21] J. C. Almeida, M. Rangel, G. Rey, Mario Pacione, C. López, and A. Valdivieso. "Well of the Future: A New Approach to Real-Time Wellbore Stability Monitoring in the Colombian Foothills". In: *SPE/IADC Drilling Conference and Exhibition* (Mar. 17, 2015). DOI: 10.2118/173129-ms.

[22] Salim Taoutaou, Cinto Azwar, Rakesh Pathak, Degaul Nzoutchoua Nana, and Prakash Anand Ajwani. "Ensuring Well Integrity in Deepwater using a fit for Purpose Advanced Cement System". In: *SPE Asia Pacific Oil and Gas Conference and Exhibition*. SPE, Sept. 20, 2011. DOI: 10.2118/147550-ms.

[23] Kaushik Manikonda, Abu Rashid Hasan, Nazmul H Rahmani, Omer Kaldirim, Chinemerem Edmond Obi, Jerome J Schubert, and Mohammad Azizur Rahman. "A gas kick model that uses the thermodynamic approach to account for gas solubility in synthetic-

based mud". In: *SPE/IADC Middle East drilling Technology conference and exhibition*. SPE. 2021, D031S016R001.

[24] Mitch Guinn and Craig Castille. "Advances in Global Industry Response Capability for Source Control". In: *International Oil Spill Conference Proceedings* 2021.1 (May 1, 2021). DOI: 10.7901/2169-3358-2021.1.688651.

[25] A. A. Ahmed, P.. Dwivedi, and Mario Ardila. "Integrated Methodology for Production and Facilities Analysis to Optimize Barnett Shale Gas Production - A Case Study". In: *Abu Dhabi International Petroleum Exhibition and Conference*. SPE, Nov. 9, 2015. DOI: 10.2118/177567-ms.

[26] A. Manzella. "Geothermal energy". In: *EPJ Web of Conferences* 148 (July 24, 2017), pp. 12–00012. DOI: 10.1051/epjconf/201714800012.

[27] Yujiang He and Xianbiao Bu. "Performance of a hybrid heating system based on enhanced deep borehole heat exchanger and solar energy". In: *Geothermal Energy* 10.1 (Oct. 28, 2022). DOI: 10.1186/s40517-022-00236-0.

[28] Claudia Gruber, Hermann F. Spoerker, and Wilhelm Brandstaetter. "Dynamic Modeling of Gas Distribution in the Wellbore During Kick Situations: The Solutions". In: *IADC/SPE Drilling Conference and Exhibition* (Mar. 4, 2014). DOI: 10.2118/167931-ms.

[29] Wenan Sun, Zhongcong Zhao, Junjie Xiong, Yujian Rong, Jin Bao, Baolei Liu, and Zhihao Chen. "A noncrosslinked <scp> CO ₂ </scp> foam fracturing fluid with low friction". In: *The Canadian Journal of Chemical Engineering* 101.5 (Oct. 13, 2022), pp. 2510–2517. DOI: 10.1002/cjce.24624.

[30] *Natural gas productive capacity for the lower 48 states 1985 through 1997*. Dec. 1, 1996. DOI: 10.2172/426976.

[31] Doru Bogdan Stoica, Cristian Nicolae Eparu, Adrian Neacsa, Alina Petronela Prundurel, and Bogdan Nicolae Simescu. "Investigation of the gas losses in transmission networks". In: *Journal of Petroleum Exploration and Production Technology* 12.6 (Dec. 29, 2021), pp. 1665–1676. DOI: 10.1007/s13202-021-01426-5.

[32] Bambang Widarsono, Heru Atmoko, Fakhriyadi Saptono, Tunggal Tunggal, and Ridwan Ridwan. "Fuzzy Logic As A Tool For Estimating Production Potential Of A Sand Layer". In: *Scientific Contributions Oil and Gas* 27.3 (Mar. 30, 2022), pp. 3–11. DOI: 10.29017/scog.27.3.872.

[33] Vicente Casariego. *Generation, Migration, and Transportation of Gas Contaminated Regions of Drilling Fluid*. Jan. 1, 1987. DOI: 10.31390/gradschool_disstheses.4438.

[34] George Koperna, Vello Kuuskraa, David Riestenberg, Aiysha Sultana, and Tyler Van Leeuwen. *Rigorous Screening Technology for Identifying Suitable CO2 Storage Sites II*. June 1, 2009. DOI: 10.2172/1039659.

[35] Earl D. Mattson and Larry Hull. *Documentation of INLs In Situ Oil Shale Retorting Water Usage System Dynamics Model*. Dec. 1, 2012. DOI: 10.2172/1070124.

[36] Kent Perry. *Counter-Rotating Tandem Motor Drilling System*. Apr. 30, 2009. DOI: 10.2172/970600.

[37] Mike Okot, Marlio Campos, German Muñoz, Alawi Alalsayednassir, Matt Weber, and Zahid Muneer. "Utilization of an Innovative Tool to Improve Hole Cleaning Efficiency in Extended Reach Wells in Saudi Arabia". In: *SPE Kuwait Oil and Gas Show and Conference*. SPE, Oct. 11, 2015. DOI: 10.2118/175165-ms.

[38] *Development of a natural Gas Systems Analysis Model (GSAM). Annual report*. Feb. 1, 1994. DOI: 10.2172/10143716.

[39] Baojin Wang, Liuci Wang, Xiangbo Meng, and Fushen Ren. "Effect of Annular GasLiquid Two-Phase Flow on Lateral Vibration of Drill String in Horizontal Drilling for

Natural Gas Hydrate". In: *Processes* 11.1 (Dec. 26, 2022), pp. 54–54. DOI: 10.3390/pr11010054.

[40] *Final Rulison Path Forward*. June 1, 2010. DOI: 10.2172/1110228.

[41] *Geothermal Energy Research and Development Program; Project Summaries*. Mar. 1, 1994. DOI: 10.2172/860862.

[42] Thomas W. Pfeifle, Francis D. Hansen, and David L. Lord. *Parameter justification report for DRSPALL*. Oct. 1, 2003. DOI: 10.2172/918329.

[43] *Utilization of coal mine methane for methanol and SCP production. Topical report, May 5, 1995–March 4, 1996*. Dec. 31, 1998. DOI: 10.2172/565265.

[44] Yankun Ma, Longyong Shu, Hongyan Li, Cong Cui, Yang Zhou, and Yang Li. "Numerical Investigation of Safety Strategy for Gas Disaster Prevention in Successive Panels Using Upper Protective Layer Mining: A Case Study." In: *International journal of environmental research and public health* 19.7 (Apr. 6, 2022), pp. 4408–4408. DOI: 10.3390/ijerph19074408.

[45] J.R. Kelsey. *Geothermal Technology Development Program. Annual progress report, October 1983-September 1984*. Aug. 1, 1985. DOI: 10.2172/5047660.

[46] Chen Wei and Yuanhang Chen. "Data Assimilation-Based Real-Time Estimation of Downhole Gas Influx Rate and Void Fraction Distribution in a Drilling Riser". In: *Volume 10: Petroleum Technology*. American Society of Mechanical Engineers, June 5, 2022. DOI: 10.1115/omae2022-79176.

[47] T.R. Farris and T.D. Jarecki. *Operability test procedure for rotary mode core sampling system number$_s$ign*3. Apr. 26, 1995. DOI: 10.2172/61112.

[48] "APPEA Conference 2003: Abstracts of Technical, Commercial and Environmental Papers and Posters". In: *The APPEA Journal* 43.1 (June 30, 2003), pp. 1–39. DOI: 10.1071/ajv43n1_abstracts.

[49] W.K. Overbey, R.S. Carden, C.D. Locke, and S.P. Salamy. *Drilling, completion, stimulation, and testing of Hardy HW[number sign]1 well, Putnam County, West Virginia*. Mar. 1, 1992. DOI: 10.2172/6910867.

[50] Miaomiao Meng, Jinqiang Liang, Zenggui Kuang, Jinfeng Ren, Yulin He, Wei Deng, and Yuehua Gong. "Distribution Characteristics of Quaternary Channel Systems and Their Controlling Factors in the Qiongdongnan Basin, South China Sea". In: *Frontiers in Earth Science* 10 (June 2, 2022). DOI: 10.3389/feart.2022.902517.

[51] R.M. Boger. *Report on Testing to Expand the Rotary Mode Core Sampling Operating Envelope*. Dec. 13, 1999. DOI: 10.2172/798805.

[52] P. Cavanagh, D. Stiles, S. Lemp, and K. Faurschou. "New Cementing Technology Eliminates Remediation, Reduces Risk and Lowers Well Costs in the Deep Foothills of Western Alberta". In: *Journal of Canadian Petroleum Technology* 43.06 (June 1, 2004), pp. 45–51. DOI: 10.2118/04-06-02.

[53] Richard P. Holst. "Preparing for LNG: A Montney Gas Field Optimization Workflow". In: *SPE/CSUR Unconventional Resources Conference*. SPE, Oct. 20, 2015. DOI: 10.2118/175939-ms.

[54] D.. Rizkiani et al. "Drilling Optimization to Overcome High Torque Problem: Lesson Learned on Kujung First Offshore-Near HPHT-Horizontal-Critical Sour-Slim Hole Development". In: *SPE/IATMI Asia Pacific Oil & Gas Conference and Exhibition*. SPE, Oct. 17, 2017. DOI: 10.2118/186954-ms.

[55] Xiangwei Kong, Yuanhua Lin, Yijie Qiu, Hongjun Zhu, Long Dong, and Yanchao Chen. "A New Model for Predicting Dynamic Surge Pressure in Gas and Drilling Mud Two-Phase Flow during Tripping Operations". In: *Mathematical Problems in Engineering* 2014.1 (Jan. 8, 2014), pp. 1–16. DOI: 10.1155/2014/916798.

[56] Claire Henderson, Harish Radhakrishna Acharya, Hope Matis, Hareesh Kommepalli, Brian Christopher Moore, and Hua Wang. *Cost Effective Recovery of Low-TDS Frac Flowback Water for Re-use*. Mar. 31, 2011. DOI: 10.2172/1030557.

[57] E.H. Ahrens and F.D. Hansen. *Large-scale dynamic compaction demonstration using WIPP salt: Fielding and preliminary results*. Oct. 1, 1995. DOI: 10.2172/188536.

[58] Umesh Javiya, John W. Chew, Nicholas J. Hills, and Timothy Scanlon. "A Comparative Study of Cascade Vanes and Drilled Nozzle Designs for Pre-Swirl". In: *Volume 5: Heat Transfer, Parts A and B*. ASMEDC, Jan. 1, 2011, pp. 913–920. DOI: 10.1115/gt2011-46006.

[59] Lin Zhang, Chengmin Wei, Yao Nie, and Ruiying Wang. "Pressure Measurement of Coal Seam with Active Nitrogen Injection: Model and Experimental Analysis." In: *ACS omega* 7.50 (Dec. 6, 2022), pp. 46935–46945. DOI: 10.1021/acsomega.2c06012.

[60] Jihad Kadhim AbdAli and Maysoon Khazaal Abbas Maaroof. "Phase Change Analysis of Robot Laser Drilling with Accuracy Enhancement by Deep Learning". In: *International Journal of Analytical, Experimental and Finite Element Analysis (IJAEFEA)* 9.3 (July 17, 2022). DOI: 10.26706/ijaefea.3.9.2211163.

[61] Yiyu Lu, Zhe Zhou, Zhaolong Ge, Xinwei Zhang, and Qian Li. "Research on and Design of a Self-Propelled Nozzle for the Tree-Type Drilling Technique in Underground Coal Mines". In: *Energies* 8.12 (Dec. 17, 2015), pp. 14260–14271. DOI: 10.3390/en81212426.

[62] Antonio C.V.M. Lage, Gabriel Sotomayor, Angela C. Vargas, Roberto Rodrigano, P. R. Silva, Humberto L. Lira, and Paulo Silva Filho. "Planning, Executing and Analyzing the Productive Life of the First Six Branches Multilateral Well Drilled Underbalanced in Brazil". In: *IADC/SPE Underbalanced Technology Conference and Exhibition*. SPE, Mar. 25, 2003. DOI: 10.2118/81620-ms.